Quantum dislocations: the fate of multiple vacancies in two-dimensional solid ^{4}He

2010 J. Phys.: Condens. Matter 22 145401

(http://iopscience.iop.org/0953-8984/22/14/145401)

J. Phys.: Condens. Matter **22** (2010) 145401 (10pp) doi:10.1088/0953-8984/22/14/145401

Quantum dislocations: the fate of multiple vacancies in two-dimensional solid ^{4}He

M Rossi, E Vitali[1], D E Galli and L Reatto

Dipartimento di Fisica, Università degli Studi di Milano, via Celoria 16, 20133 Milano, Italy

E-mail: maurizio.rossi@unimi.it

Received 23 December 2009
Published 17 March 2010
Online at stacks.iop.org/JPhysCM/22/145401

Abstract

Defects are believed to play a fundamental role in the supersolid state of ^{4}He. We have studied solid ^{4}He in two dimensions (2D) as a function of the number of vacancies n_v, up to 30, inserted in the initial configuration at $\rho = 0.0765$ Å^{-2}, close to the melting density, with the exact zero-temperature shadow path integral ground state method. The crystalline order is found to be stable also in the presence of many vacancies and we observe two completely different regimes. For small n_v, up to about 6, vacancies form a bound state and cause a decrease of the crystalline order. At larger n_v, the formation energy of an extra vacancy at fixed density decreases by one order of magnitude to about 0.6 K. It is no longer possible to recognize vacancies in the equilibrated state because they mainly transform into quantum dislocations and crystalline order is found almost independently of how many vacancies have been inserted in the initial configuration. The one-body density matrix in this latter regime shows a non-decaying large distance tail: dislocations, that in 2D are point defects, turn out to be mobile, their number is fluctuating, and they are able to induce exchanges of particles across the system mainly triggered by the dislocation cores. These results indicate that the notion of the incommensurate versus the commensurate state loses meaning for solid ^{4}He in 2D, because the number of lattice sites becomes ill defined when the system is not commensurate. Crystalline order is found to be stable also in 3D in the presence of up to 100 vacancies.

(Some figures in this article are in colour only in the electronic version)

1. Introduction

Solid ^{4}He has been the subject of many experimental and theoretical studies [1–3] since the discovery of non-classical rotational inertia [4] (NCRI), an expected manifestation of supersolidity [5]. Supersolidity is a new state of matter in which spatial order and off-diagonal long range order (ODLRO) are present at the same time, implying some forms of superfluid properties, and was already predicted long ago [6, 7]. This novel state of matter attracts interest also as regards the prospect of finding it in cold atoms in optical lattices [8]. However the precise nature of solid ^{4}He at low temperature is still elusive. Experimental evidence suggests that defects play an important role in NCRI, but which kind of disorder is responsible for the anomalous properties of solid ^{4}He is still not clear. Many different defects have been considered, but none of the proposed models has proved able to capture all the phenomenology of supersolidity. For example the stiffening of ^{4}He below the 'transition' temperature [9] suggests dislocations as a candidate, but this possibility has difficulty in explaining the NCRI seen in solid ^{4}He in Vycor [4] or in aerogel [10]. Grain boundaries have been considered too [1], but NCRI has been observed also in single crystals [11].

Defected solid ^{4}He systems have been studied by means of quantum Monte Carlo (QMC) techniques [12–23]. Such QMC methods are by construction equilibrium methods, so defects have to be stabilized by periodic boundary conditions (via a suitable choice of the simulation box) or by fixing the degrees of freedom of a number of atoms surrounding the defect of interest. This constraint on the configurational space usually does not prevent the study of the physical properties of the defected system, and the results are generally in a good quantitative agreement with experimental observations; see, for example, the estimation of the vacancy activation

[1] Present address: INFM–CNR DEMOCRITOS National Simulation Center, via Beirut 2-4, 34014 Trieste, Italy.

energy [12] or the binding energy of a ^{3}He atom to the dislocation core [22]. Exact QMC results, both at finite [17–19] and at zero temperature [24], show that two and three vacancies form a bound state. A systematic study of many vacancies in solid ^{4}He is still lacking; questions like whether the crystalline structure is stable in the presence of a large number of vacancies, whether the vacancy–vacancy interaction is pairwise additive (or almost so), whether many vacancies lead to phase separation as suggested in [17, 19], or whether vacancies turn themselves into other kinds of defects are, in our view, still unanswered.

Since the earliest days of supersolidity, quantum lattice models have been considered [25]. A terminology borrowed from lattice models is currently used for solid ^{4}He in terms of a commensurate state (i.e. a perfect crystal in which there are an integer number of atoms per unit cell) or an incommensurate one (a crystal with non-integer probability of occupation of the unit cell). QMC at $T = 0$ K for solid ^{4}He with one or a few vacancies in the simulation cell beautifully [16] confirms the picture of an incommensurate state: the vacancy (vacancies) is (are) mobile and the number of density maxima is equal to the number of particles *plus* the number of vacancies. But are we sure that we understand vacancies at a finite concentration in a macroscopic system? Is the option commensurate or incommensurate really appropriate for solid ^{4}He? One should keep in mind that in a lattice model or in cold atoms in an optical lattice the lattice periodicity is externally imposed, whereas in solid ^{4}He the same dynamical entities, the atoms, have to build up the periodicity as well as the delocalization required for supersolidity. This 'mermaid' aspect of the atoms is unique to a quantum solid. The purpose of this paper is to address such issues with exact QMC methods at $T = 0$ K in two dimensions (2D).

We find that size and box commensuration effects are very pronounced, so in order to be able to explore very large distances in a Monte Carlo calculation, up to 100 Å, we have mainly studied solid ^{4}He in 2D. In this context, the 2D solid is also of interest as a simple model for out of registry solid ^{4}He adsorbed on planar substrates, such as graphite or silica glasses. New experimental investigations [26] are under way to answer the question of whether a supersolid state is present also in adsorbed ^{4}He. We have studied 2D solid ^{4}He systems at $T = 0$ K with a number of atoms up to and above thousand containing up to 30 vacancies. We find that crystalline order is stable also in the presence of a large number of vacancies, at least in the range $\lesssim$2.5% of vacancy concentration studied by us. Multiple vacancies are highly correlated with a preference to form linear structures, but in the presence of 10 or more vacancies the scars in the lattice are healed away, transforming the vacancies mainly into dislocations. Such dislocations are not permanent structures, but are mobile and their number is fluctuating. This allows the exchange of particles across the system, not only in the cores of dislocations, giving the possibility of establishing a well defined, at least locally, phase [27], and indeed, in the simulated systems, we find a non-decaying large distance tail in the one-body density matrix. This hints at the possibility that an extended system is supersolid, but more work is needed to corroborate this conclusion.

We do not address here the origin of vacancies/dislocations, i.e. whether the true ground state of solid ^{4}He contains or does not contain zero-point defects. Our finding is that solid ^{4}He, at least in 2D, is much more complex than the picture derived from the notion of a commensurate versus an incommensurate state, because the number of lattice sites is an ill defined quantity when dislocations are present. The number of lattice sites is a meaningful quantity, at least for the sizes that we are able to simulate, only if the number of particles and the simulation box are such that the regular lattice exactly fits in or the misfit is limited to just one or very few vacancies. We have performed few simulations also in three dimensions (3D). Also in this case we find that, near melting, crystalline order is stable even in the presence of 100 vacancies, but we have not yet performed a detailed characterization of the disorder in the system.

The paper is organized as follows. Section 2 deals with the exact $T = 0$ K SPIGS method. Details of the simulations are outlined in section 3. Section 4 contains our results and our conclusions are given in section 5.

2. The SPIGS method

We employ the exact $T = 0$ K shadow path integral ground state (SPIGS) [15] method, an 'exact' QMC technique [28, 29]. SPIGS is an extension of the path integral ground state (PIGS) [30] method. The aim of PIGS is to improve a variationally optimized trial wavefunction ψ_T by constructing a path in the Hilbert space of the system which connects the given ψ_T to the lowest energy state of the system, ψ_0, constrained by the choice of the number of particles N, the geometry and the boundary conditions of the simulation box and the density ρ. During this 'path', the correct correlations among the particles arise through the 'imaginary time evolution operator' $e^{-\tau\hat{H}}$, where $\hat{H}$ is the Hamiltonian operator. For a large enough τ, an accurate representation for the lowest energy state wavefunction is given by $\psi_\tau = e^{-\tau\hat{H}}\psi_T$, which can be written analytically by discretizing the path in imaginary time and exploiting the factorization property $e^{-(\tau_1+\tau_2)\hat{H}} = e^{-\tau_1\hat{H}}e^{-\tau_2\hat{H}}$. In this way, ψ_τ turns out to be expressed in terms of convolution integrals which involve the 'imaginary time propagator' $\langle R|e^{-\delta\tau\hat{H}}|R'\rangle$ for small $\delta\tau$, for which very accurate approximations can be found in the literature [31, 32]. This maps the quantum system into a classical system of open polymers [30]. An appealing feature peculiar to the PIGS method is that, in ψ_τ, the variational ansatz acts only as a starting point, while the full path in imaginary time is governed by $e^{-\tau\hat{H}}$, which depends only on the Hamiltonian operator. We have recently shown that PIGS results for large enough τ are unaffected by the choice of ψ_T both in the liquid and in the solid phase [28, 29], thus providing an unbiased exact $T = 0$ K QMC method. Within SPIGS, a shadow wavefunction (SWF) [33, 34] is taken as ψ_T and this choice was shown to greatly accelerate convergence to ψ_0. Another appealing feature of the SPIGS method is that it recovers the solid phase via a spontaneously broken translational symmetry [15] and there is no constriction on

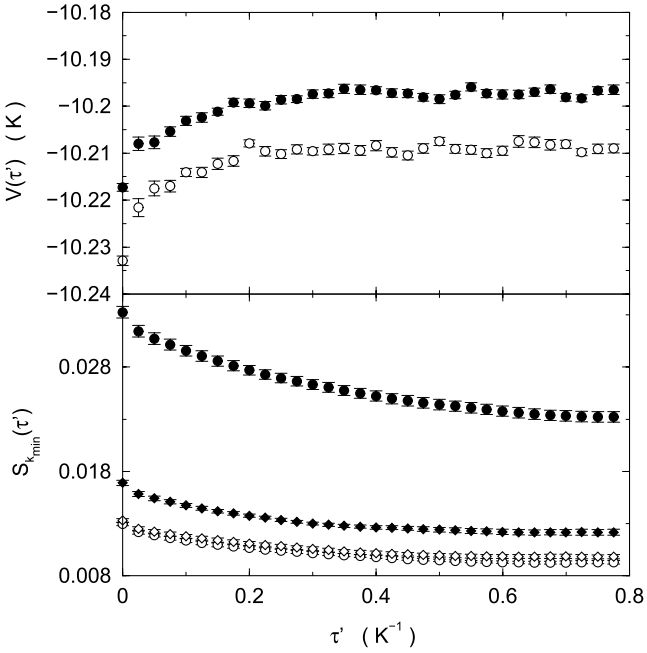

Figure 1. Upper panel: mixed expectation value for the potential energy per particle as a function of the projection time τ' computed for a 2D ^{4}He crystals at $\rho = 0.0765$ Å^{-2} in the $M = 960$ box, with $n_v = 0$ (open symbols) and $n_v = 20$ (filled symbols). Lower panel: static structure factor computed for the same systems for the lowest wavevectors along the first-neighbor direction (circles, $k_{min} = 0.055$ Å^{-1}) and orthogonal to the first-neighbor direction (diamonds, $k_{min} = 0.059$ Å^{-1}). Open and filled symbols have the same meaning as in the upper panel.

the atomic positions, so it is particularly indicated in studying crystals with defects.

3. The model system and simulation details

By studying the equation of state we find the freezing and the melting densities to be, respectively, $\rho_f = 0.0672$ Å^{-2} and $\rho_m = 0.0724$ Å^{-2}. As the simulation box we choose then a rectangular box fitting a regular triangular lattice with M lattice sites at $\rho = 0.0765$ Å^{-2}. Periodic boundary conditions (pbc) are applied in both directions. Dealing with low temperature properties, ^{4}He atoms are described as structureless zero-spin bosons, interacting through the HFDHE2 Aziz potential [35]. In order to avoid any approximation associated with the estimation of tail corrections due to the finite size of the simulation boxes, we have considered a truncated and shifted Aziz potential which goes to zero at $r_{cut} = 6$ Å. Since r_{cut} is well below the minimum size of each box considered, the results relating to different box sizes can be compared without any further correction. Our SPIGS computation is based on the pair-product approximation for the imaginary time projector [31] and the imaginary time step $\delta\tau = 1/40$ K^{-1} has been chosen in order to ensure a good accuracy and a reasonable computational effort [28].

An important parameter in the computation is the total projection time τ. Any trial wavefunction ψ_T can be expanded in terms of the exact ground state and of the excited states of zero total linear momentum. If we call the minimum excitation energy for such excited states $\Delta\varepsilon_{min}$, τ has to be larger than $(\Delta\varepsilon_{min})^{-1}$ in order to project out any excitation contribution in ψ_T; the rate of rejection of such contributions depends also on the quantity that one is computing due to the sensitivity to missing long range correlations in ψ_T or to wrong short range correlations. For the perfect crystal, using K as the energy unit, $\tau = 0.775$ K^{-1} was found [28] to be large enough to ensure convergence of both diagonal and off-diagonal observables when a SWF is used as ψ_T. This is compatible with the criterion $\tau > (\Delta\varepsilon_{min})^{-1}$. In fact, the lowest energy excitations in a perfect crystal are phonons; thus $\Delta\varepsilon_{min}$ corresponds to the combination of two phonons of opposite $\vec{k}$ with the smallest achievable k value, i.e. in a box with pbc $k_{min} = 2\pi/L_{max}$ where L_{max} is the largest side. Via a new analytic continuation method [36] we have estimated the longitudinal sound velocity for 2D solid ^{4}He at $\rho = 0.0765$ Å^{-2} to be $c = 36.5 \pm 2.5$ K Å. Then the minimum imaginary time required for convergence is $\tau_{min} = 1/\Delta\varepsilon_{min} \simeq 0.25$ K^{-1} in the largest simulation box considered here. This value is well below the one used, $\tau = 0.775$ K^{-1}. Since the transverse sound velocity is typically similar to c, the τ value considered is enough to ensure also the removal of transverse phonon contributions. The situation might be different in the presence of vacancies, or other kinds of defects, because novel low energy excitation modes could be present. We have performed several tests in order to become confident that the value of τ considered is large enough also for defected crystals. The most straightforward test is to perform simulations with larger τ values and verify that the expectation values are compatible within the statistical uncertainty. Such a test turns out to be very time-consuming and in practice it has been feasible only for a number of ^{4}He atoms $N \lesssim 250$, where we have increased the value of τ up to 1.16 K^{-1} finding good convergence for diagonal properties. An indirect test for the convergence is provided by the behavior of suitably chosen observables on the imaginary time path. If we define

$$\mathcal{O}(\tau') = \frac{\langle\psi_{\tau'}|\hat{\mathcal{O}}|\psi_{2\tau-\tau'}\rangle}{\langle\psi_{\tau'}|\psi_{2\tau-\tau'}\rangle} \qquad (1)$$

for $0 \leqslant \tau' \leqslant \tau$, when τ is large enough, we have $\psi_{2\tau-\tau'} \simeq \psi_0$ and equation (1) gives the mixed expectation value $\mathcal{O}(\tau') = \langle\psi_{\tau'}|\hat{\mathcal{O}}|\psi_0\rangle/\langle\psi_{\tau'}|\psi_0\rangle$ as a function of the partial imaginary time τ'. If $\mathcal{O}(\tau')$ has a plateau when $\tau' \to \tau$, it is guaranteed that τ is large enough for convergence and the plateau represents the 'exact' expectation value of $\hat{\mathcal{O}}$. A couple of examples are shown in figure 1 for the potential energy ($\hat{\mathcal{O}} = \hat{V}$) and for the static structure factor at the lowest wavevectors ($\hat{\mathcal{O}} = \hat{\rho}_{-k_{min}}\hat{\rho}_{k_{min}}$, where $\hat{\rho}_{\vec{k}} = \frac{1}{\sqrt{N}}\sum_{j=1}^{N}\exp(i\vec{k}\cdot\vec{r}_j)$ is the density fluctuation operator) along the simulation box axis. As far as the potential energy V is concerned, excitation modes are rapidly projected out and $\tau \simeq 0.25$ K^{-1} is enough for achieving convergence both in the perfect and in the defected systems, as shown in figure 1 by the presence of a plateau of $V(\tau')$ in both cases. Larger values of the imaginary time are needed to reach convergence for quantities that depend on long range correlations, such as the static structure factor at small

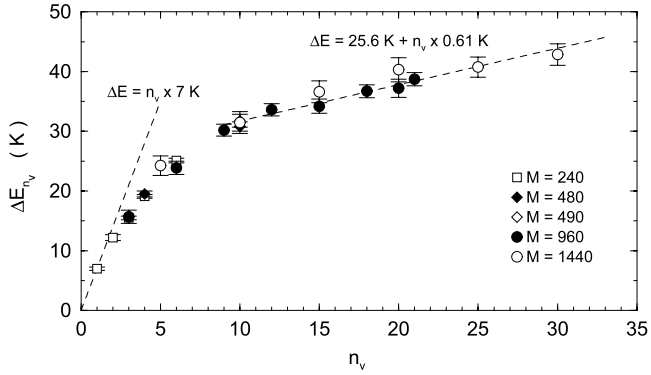

Figure 2. Defect formation energy ΔE_{n_v} as a function of n_v in 2D solid ^{4}He at $\rho = 0.0765$ Å^{-2} computed in boxes with different lattice site numbers, M. Dashed lines are linear fits to the data.

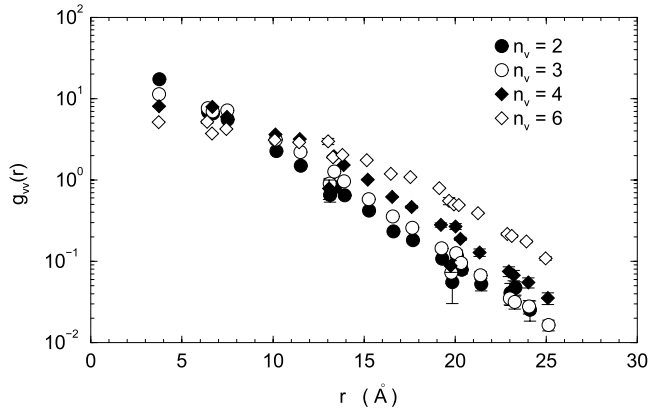

Figure 3. Vacancy–vacancy correlation function $g_{\mathrm{vv}}(r)$ computed for 2D solid ^{4}He at $\rho = 0.0765$ Å^{-2} in a box with $M = 240$ lattice sites for different numbers of vacancies n_v. $g_{\mathrm{vv}}(r)$ is normalized with the correlation function for n_v vacancies randomly distributed on the same lattice.

wavevectors ($S_{k_{\mathrm{min}}}$) [37]. For the perfect crystal, convergence for $S_{k_{\mathrm{min}}}$ is achieved at about 0.6 K^{-1}, as shown in figure 1. For the defected crystal (especially when many vacancies are present as in the case considered in the figure), the chosen $\tau = 0.775$ K^{-1} value is just enough for getting convergence. An interesting physical effect emerges from figure 1: the static structure factor is strongly affected by the presence of defects especially along the nearest neighbor direction.

Two independent simulations are needed in order to calculate the formation energy of n_v vacancies, one with $N = M$ particles (the regular ideal crystal, dubbed also the perfect crystal), and one with n_v fewer atoms (the defected crystal). In this second case we say that we have $n_\mathrm{v} = M - N$ vacancies, even if in general we can talk of vacancies only in the starting configuration of the simulation, where n_v atoms are removed from the perfect lattice. In fact, in SPIGS, like in PIMC, there is no constraint on the atomic positions, so vacancies are free to transform into different kinds of defects. In the presence of vacancies, after removing n_v particles from the ideal starting configuration, we rescale the dimensions of the simulation box to reset the system to the original density. This

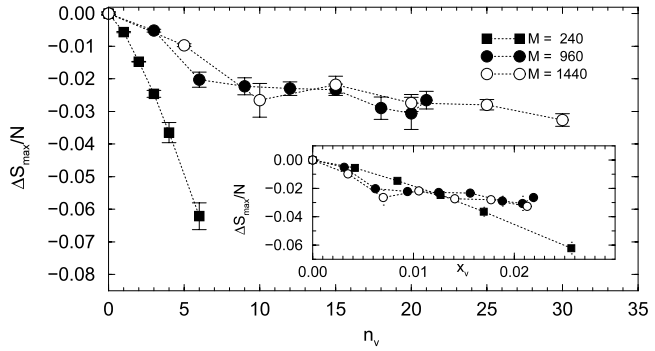

Figure 4. $\Delta S_{\mathrm{max}}/N = S_{\mathrm{max}}^{n_\mathrm{v}}/(M - n_\mathrm{v}) - S_{\mathrm{max}}^{n_\mathrm{v}=0}/M$ as a function of the number of vacancies n_v (and of the concentration of vacancies x_v in the inset) for different M values. $S_{\mathrm{max}}^{n_\mathrm{v}}$ is the main Bragg peak integrated intensity (see footnote 5). The main Bragg peak is at $|\vec{k}| \simeq 1.87$ Å^{-1}. Lines are an aid to the eyes.

is performed to circumvent the need for correcting the energy due to density changes caused by the inclusion of vacancies. The formation energy of n_v vacancies is proportional to the difference [12][2] between the energy per particle of the defected crystal, $e(M - n_\mathrm{v})$, and that for the perfect one, $e(M)$, i.e.

$$\Delta E_{n_\mathrm{v}} = (M - n_\mathrm{v})[e(M - n_\mathrm{v}) - e(M)]. \tag{2}$$

When vacancies turn into dislocations this ΔE_{n_v} has the meaning of a defect formation energy at fixed density. One can consider also the formation energy $\Delta \tilde{E}_{n_\mathrm{v}}$ at a fixed lattice parameter; this is given by

$$\Delta \tilde{E}_{n_\mathrm{v}} = \Delta E_{n_\mathrm{v}} - n_\mathrm{v}\mu, \tag{3}$$

μ being the chemical potential, that for our system turns out to be $\mu = 14.22 \pm 0.02$ K.

We check the presence of crystalline order by monitoring the static structure factor for the presence of Bragg peaks. In addition, we compute the particle coordination number, via a Delaunay triangulation[3] (DT) of the sampled configurations, in order to estimate the amount of disorder in the system [38]. In a perfectly ordered 2D triangular crystal each atom is linked to six other atoms in the DT. Atoms with coordination number not equal to 6 are then a measure of the disorder in the crystal [38]. A conservation law exists for the coordination numbers [38]:

$$\sum_{i=3}^{5}(6 - i)N_i = \sum_{i=7}^{\infty}(i - 6)N_i \tag{4}$$

where N_i is the number of i-coordinated atoms, so we can consider only N_i with $i < 6$. Therefore we take $\tilde{X}_\mathrm{d} = 2N_4 +$

[2] Both $e(M - n_\mathrm{v})$ and $e(M)$ are ground state energies of two periodically repeated small systems, and their difference ΔE_{n_v} has been used for estimating the formation energy of extra vacancies in the bulk; therefore ΔE_{n_v} is a derived quantity [16].

[3] The Delaunay triangulation (DT) for a set P of N points in the plane is a triangulation $\mathcal{T}(P)$ such that no point in P is inside the circumcircle of any triangle in $\mathcal{T}(P)$. DT corresponds to the dual graph of the Voronoi tessellation, i.e. the partitioning of the plane into convex polygons such that each polygon contains exactly one point in P and every point of the plane closer to it than to any other point of P. Then each point in P is linked only to its nearest neighbors. The number of sides of the Voronoi polygons (of the links in DT) is the coordination number of the generating point.

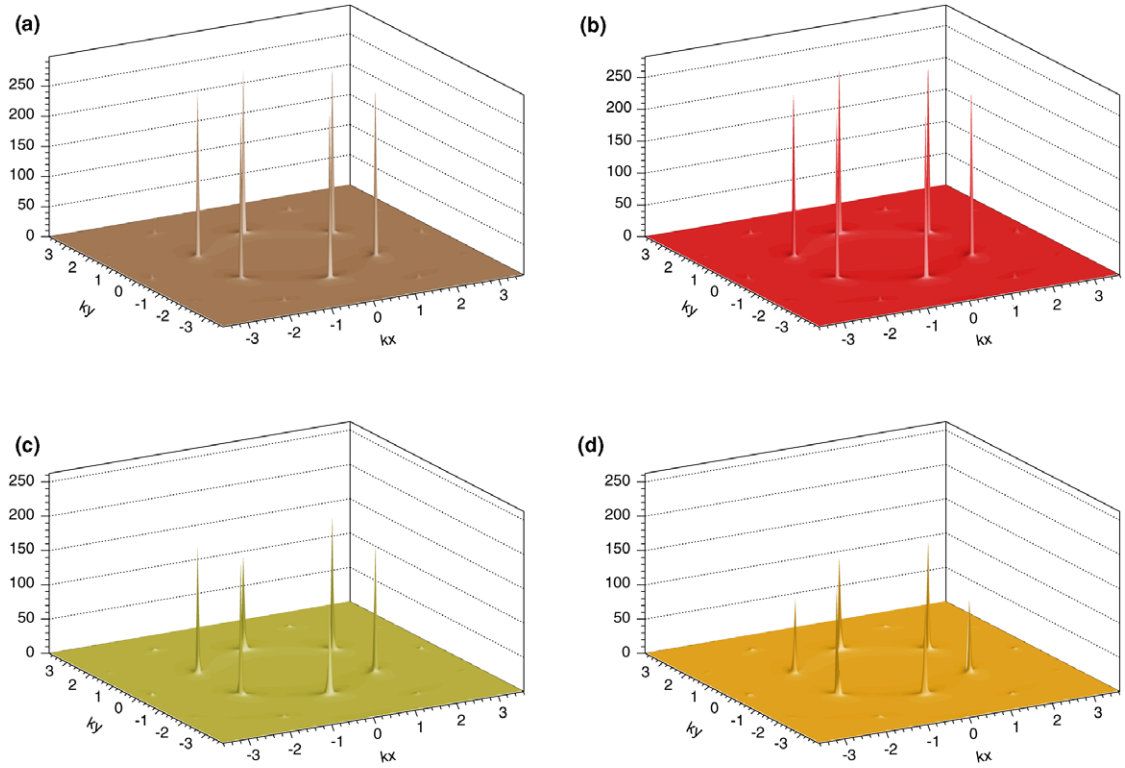

Figure 5. Static structure factor $S(\vec{k})$ in the k_x, k_y plane computed in a ^{4}He 2D crystal at $\rho = 0.0765$ Å^{-2} in a box with $M = 1440$ lattice sites and with different n_v values. The wavevectors are in Å^{-1}. (a) $n_v = 0$; (b) $n_v = 5$; (c) $n_v = 15$; (d) $n_v = 25$.

N_5 as an estimate of disorder in the system (we never found three-sided polygons, i.e. $N_3 = 0$). For a perfect ($N = M$) 2D quantum crystal the coordination is 6 only on average; in fact, due to the large zero-point motion, fluctuations are present such that atoms do not have always coordination 6. Thus, a more useful quantity measuring the net amount of disorder in a crystal with defects is the difference between the observed $\tilde{X}_d$ and that of the corresponding perfect crystal:

$$X_d = (2N_4 + N_5)_M^{n_v} - (2N_4 + N_5)_M^{n_v=0}. \quad (5)$$

When the number of vacancies n_v is small, up to 6, we have also computed the vacancy–vacancy correlation function $g_{vv}(r)$ by recording the relative distances among vacancies during the Monte Carlo sampling. The determination of the vector positions of the vacancies in a crystalline configuration is far from being trivial due to the large zero-point motion, due to high vacancy mobility and because in our algorithm the center of mass is not fixed. Vacancy positions are obtained via the coarse-graining procedure illustrated in [24]. This method is efficient as long as we have few vacancies. For large n_v the efficiency in recognizing the position of vacancies becomes extremely poor (in fact, as we shall see, vacancies turn into dislocations); then is no longer possible to compute $g_{vv}(r)$. Different definitions of vacancy positions, like the one in [18], give very similar results[4].

[4] The algorithm proposed in [18] by construction provides always $n_v = M - N$ vacancy positions. For few vacancies the results with this algorithm agree with those obtained with the coarse-graining method used here. When many vacancies are present (and turn into dislocations) the vacancy positions given by the algorithm of [18] are extremely erratic from one configuration to the following one and thus are not reliable.

Special care has been devoted to ruling out possible metastability effects. We have considered different starting configurations for vacancies, i.e. we have removed a number n_v of atoms forming a compact cluster or a linear cluster, or the removed atoms come from random lattice positions. After long enough equilibration (our simulations are never shorter than 6×10^5 Monte Carlo steps) we find agreeing results for systems with the same n_v value. In order to rule out possible finite size effects and pbc bias we have considered systems of increasing sizes (M values). Again we find compatible results for systems of different sizes and with equal n_v values, so no appreciable finite size effects have been detected. The only exception regards the one-body density matrix that will be discussed below. Furthermore we have considered also crystals with no principal crystalline axis parallel to the box sides, obtaining once more the same results. Moreover, we have considered systems where the starting configuration was obtained by removing n_v particles from an equilibrated configuration of the perfect crystal and at the same time the positions of one (two) line(s) of atoms, parallel to one (both) box side(s), were kept fixed during the Monte Carlo sampling. Even in these cases, the results do not change; for instance, for large n_v values, vacancies are found to turn into dislocations with the same features as in the fully mobile systems.

4. Results

We have studied a triangular crystal at $\rho = 0.0765$ Å^{-2} with $M = 240$, 480, 960 and 1440 lattice positions of the perfect crystal. Our results for the formation energy ΔE_{n_v}

at constant density are plotted in figure 2. The dependence of ΔE_{n_v} on n_v is monotonic and systematically sublinear, confirming the existence of an attractive interaction among vacancies. Systems with the same n_v and different M have the same ΔE_{n_v} within the statistical uncertainty, i.e. ΔE_{n_v} has no significant dependence on $x_v = n_v/M$, at least in the range $x_v \lesssim 2.5\%$ that we have studied. From the plot in figure 2 it is possible to recognize two different behaviors: for $n_v < 6$, ΔE_{n_v} deviates rapidly from the linear dependence and vacancies form a bound state as indicated by a (roughly) exponentially decreasing correlation function $g_{vv}(r)$, plotted in figure 3. For $n_v > 10$ the ratio $\Delta E_{n_v}/n_v$ remains practically constant with a value of about 0.61 K. This means that, when some vacancies are already present in the system, the creation of an additional vacancy has a very low cost, about one tenth of the cost of a single vacancy. Notice that in the linear regime, ΔE_{n_v}, at fixed lattice parameter, is negative; there is a *gain* of 13.61 K for each additional vacancy.

The double-regime behavior of ΔE_{n_v} is reflected also in other properties of the system, for instance in the static structure factor $S(\vec{k})$. For a finite crystal the height S_{max} of the Bragg peaks has a strong dependence on the number of particles N and S_{max}/N shows a slow convergence (like $N^{-2/3}$ in 3D [39] and $N^{-1/2}$ in 2D) to the thermodynamic limit. Note that at $T = 0$ K, the crystalline order is stable also in 2D. Our computation of S_{max}/N for the perfect crystal verifies this $N^{-1/2}$ dependence as expected for a 2D crystal. This $N^{-1/2}$ dependence of S_{max}/N arises from missing phonon modes for $k < k_{min}$ in a finite box, so essentially the same $N^{-1/2}$ contribution is expected to be present in the defected system. Therefore by taking the difference between S_{max}/N in the defected system and the value for the perfect crystal, such an $N^{-1/2}$ contribution cancels out to a large extent so we can compare results for crystals of different sizes and n_v values. Since the crystalline lattice relaxes around a vacancy, one expects the heights of the Bragg peaks in $S(\vec{k})$ to decrease with increasing number of vacancies. This is observed, as shown in figure 4, only when n_v is small. For large n_v values we find a very different behavior. The main Bragg peak height has some broadening, but its integrated intensity[5] does not show a significant dependence on n_v; rather it oscillates around an almost constant value. In figure 5 we show the static structure factor $S(\vec{k})$ in the $\vec{k}$ plane obtained for $n_v = 0$, 5, 15 and 25 in the largest box considered, with $M = 1440$ lattice sites. When the number of vacancies is small (figure 5(a)) we find Bragg peaks in the first reciprocal vector star as sharp as in the case of the perfect crystal, within the resolution $\Delta k = \frac{2\pi}{L}$ due to the finite size of the simulation box, but with a decreased height. Otherwise (see figures 5(c) and (d)), for large n_v, the Bragg peaks turn out to be slightly broadened, but their integrated intensity (see figure 4) shows no significant dependence on n_v. The broadening σ_{max} of the main Bragg peak has a linear dependence on the concentration of defects x_v, with $\sigma_{max} \simeq 1.5 \times x_v$ Å^{-1}.

[5] The broadening of the Bragg peaks occurs for a small number of close points in the k-grid (wavevectors in a finite system with pbc are quantized); thus we refer to the sum of $S(\vec{k})$ over the k-points contributing to the Bragg peak as the integrated intensity.

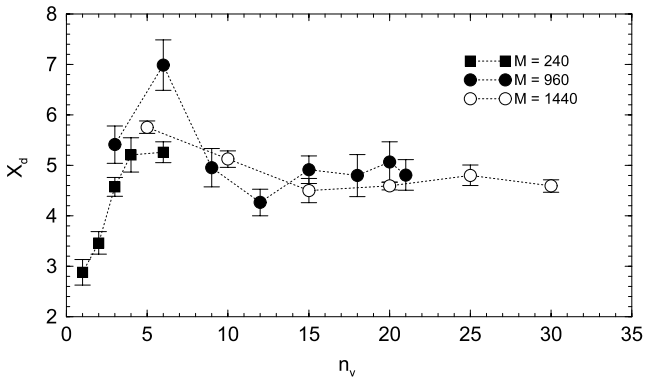

Figure 6. Amount of disorder X_d as a function of n_v. Lines are an aid to the eyes.

A similar behavior is displayed also by the amount of disorder X_d, plotted in figure 6. X_d increases with n_v for small n_v values and saturates to an almost constant value for larger n_v. By examining sampled configurations of the system in this regime, we find that it is no longer possible to identify vacancy positions. Rather one finds dislocations, as shown by a DT of the position of the atoms; see figures 7(a) and (b). Dislocation cores in 2D are point defects characterized by a couple 5–7 in the coordination number of neighboring atoms in the DT. We find that dislocations do not prefer any of the principal lattice directions. Studying a large collection of independent configurations one finds that a large fraction of them contain a couple of dislocation cores (see figure 7). For example, for $n_v = 20$ in the $M = 960$ box, there is a probability of about 90% for two dislocation cores and 10% of finding more than two dislocation cores. In addition there is a probability around 3% of finding also some isolated vacancies besides dislocations (see figure 7(c)). Similar values are found for $n_v = 20$ in the $M = 1440$ box. We stress that, even if initially placed in a compact cluster configuration, vacancies do not separate into a vacancy rich region surrounded by a regular crystal. Rather they mostly reorganize themselves across the system giving rise to dislocations. In this regime of large n_v the quantity that maintains direct physical meaning is $N = M - n_v$, the number of atoms. When atoms rearrange themselves giving rise to dislocations, the number of lattice sites becomes *ill defined* because the lattice positions of the perfect crystal compatible with the simulation box and the pbc no longer represent equilibrium positions for the particles, and it is no longer possible to recognize a regular lattice describing the equilibrium positions of the particles. Still we continue to use M, and $n_v = M - N$ as a convenient measure of deviation from the ideal crystal with $N = M$ where crystalline order is perfect. In the regime of small n_v, vacancies are strongly correlated and prefer to form linear configurations, as shown in figure 8. These linear configurations can be considered as forerunners of the quantum dislocations found at larger n_v. This behavior has some similarities with the behavior of colloidal crystals in 2D [40, 41]. We find that dislocations are not fixed structures; rather they are very mobile and their number changes during the simulation. As an example, in figure 9 we show the evolution of the DT of a configuration

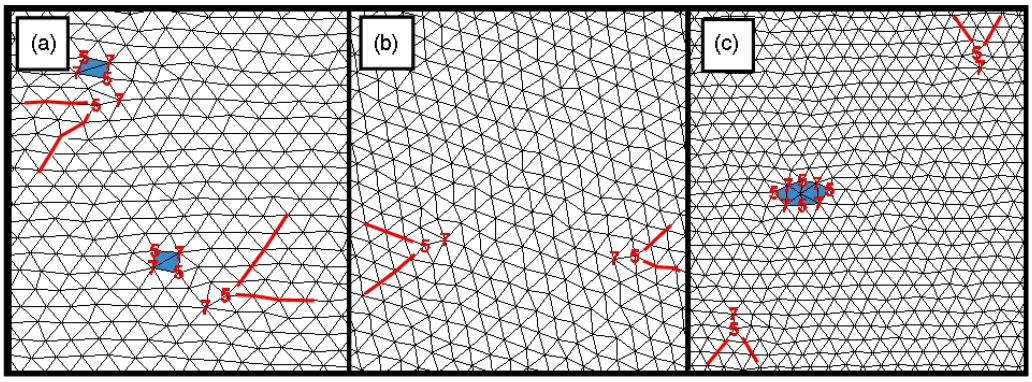

Figure 7. Delaunay triangulation of typical equilibrium configurations of a 2D ^{4}He crystal at $\rho = 0.0765$ Å^{-2} with (a) $n_v = 10$ and $M = 480$, (b) $n_v = 10$ and $M = 490$ and (c) $n_v = 20$ and $M = 1440$. The bold (red) lines indicate the interrupted lines of atoms. We report the coordination number for atoms only when different from 6. The couple 5–7 indicates a dislocation core in 2D and the clumps of two 5s and two 7s (shadowed area in panel (a)) indicate bound pairs of dislocations [38]. In (c), besides the dislocations, two close threefold-symmetric monovacancies [40] are also present (shadowed area). Notice that in all panels only a small part of the full system is shown.

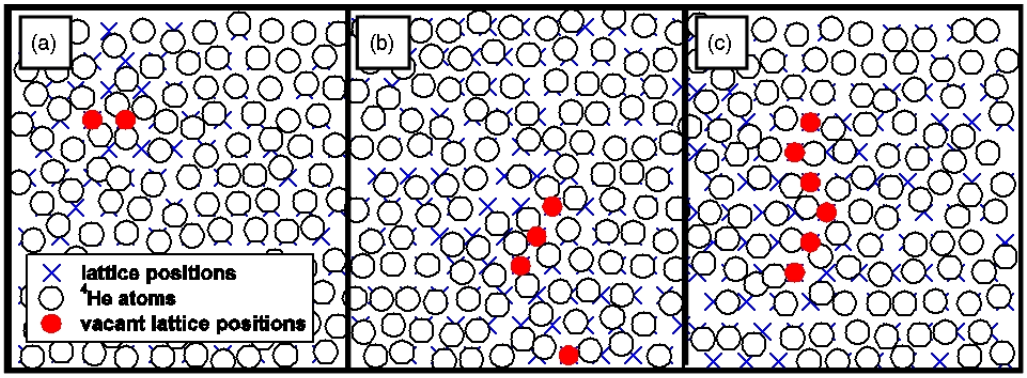

Figure 8. Vacancy configuration in a 2D ^{4}He with $M = 240$ and (a) $n_v = 2$, (b) $n_v = 4$ and (c) $n_v = 6$. Vacancy positions are obtained as in [24]. Notice that in all panels only a small part of the full system is shown.

for $n_v = 10$ vacancies in the box with $M = 480$ sampled at different Monte Carlo times.

The one-body density matrix $\rho_1(\vec{r}, \vec{r}\,')$ has a central role since the presence of a plateau at large $|\vec{r} - \vec{r}\,'|$ indicates the presence of ODLRO, i.e. the system has Bose–Einstein condensation (BEC). Even $\rho_1(\vec{r}, \vec{r}\,')$ seems to show the signature of a double-regime behavior depending on the number of vacancies. Some of our results for the one-body density matrix are reported in figure 10. As found in the 3D case [16], when only a single vacancy is present ρ_1 displays a non-zero plateau, which is the signature of ODLRO. As vacancies are added, the tail of one-body density matrix is depressed, even if it does not show a simple exponential decay. In order to be conclusive on the behavior of ρ_1 in the large distance range, one should compute it in larger systems; we have faced these computationally intensive calculations in the n_v range where vacancies give rise to quantum dislocations. Here (see figures 10(b) and 12(c)) ρ_1 displays a recognizable plateau at large distances (very evident in the largest system). In order to understand the origin of the observed off-diagonal contributions to ρ_1 in the dislocation regime it is useful to recall that in a SPIGS computation $\rho_1(\vec{r}, \vec{r}\,')$ (which is the probability amplitude for destroying a particle in $\vec{r}\,'$ and for creating one in $\vec{r}$) is obtained by splitting one of the linear polymers into two half-polymers [15], one departing from $\vec{r}$ and the other from $\vec{r}\,'$. We find that the main contribution to the plateau comes from configurations where at least one of the half-polymers occupies a dislocation core; see figures 11(a) and (b). This means that the system is able to transfer particles from one quantum dislocation to another. This is quite distinct from the observed superfluidity along the core of a screw dislocation [21] in 3D; in fact in 2D a dislocation core is a point defect and not a linear one as in 3D. Furthermore, the possibility of finding a half-polymer out of the cores like in figures 11(b) and (c) means that quantum dislocations are also able to induce vacancies in the surrounding crystal. In contrast to the diagonal properties case, in the computed one-body density matrix we find the presence of significant size effects, as can be inferred for example from the significant difference between ρ_1 for the $M = 700$, $n_v = 10$ system and that for the $M = 960$, $n_v = 20$ one, in the intermediate distance range (20–40 Å). This is shown more clearly in figure 12, where we report ρ_1 in the full plane; one can notice the presence of ridges in the tail of ρ_1 for the smaller systems ($M = 480$ and 700; see panels (a) and (b)) that are no longer present for the largest system (see figure 12(c)). Such ridges are due to an effect of commensuration with the simulation box. We have evidence that in the $M = 480$ and 700 systems, dislocation cores prefer to stay at a distance of

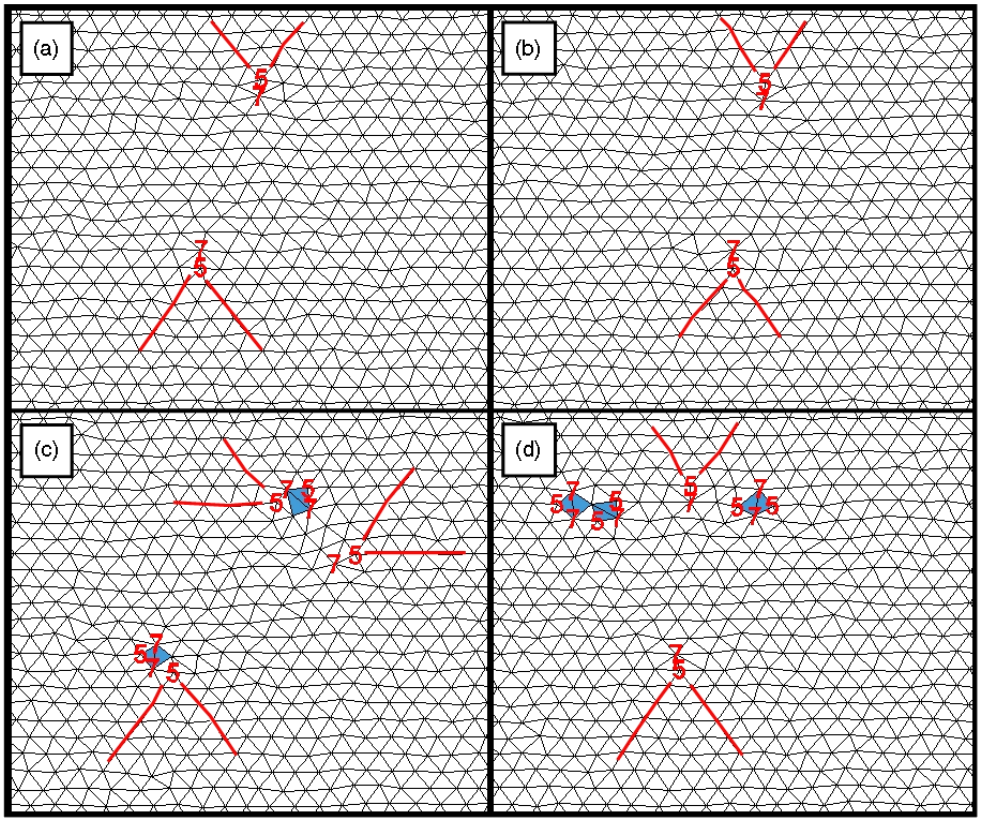

Figure 9. Example of the evolution of DT at different Monte Carlo times (MCS) in a converged computation for a 2D ^{4}He crystal at $\rho = 0.0765$ Å^{-2} with $n_v = 10$ and $M = 480$. The bold (red) lines indicate the interrupted lines of atoms. We report the coordination number for atoms only when different from 6. The couple 5–7 indicates a dislocation core in 2D. The clump of two 5s and two 7s (shadowed areas) indicates a bound pair of dislocations (BPD) [38]. Starting from the configuration shown in the panel (a), after 300 MCS, dislocation cores are found to have glided along the horizontal lattice axis by a lattice parameter (b). After 1100 MCS (c) we find three dislocation cores. Then after 1700 MCS we find again two dislocation cores, aligned along the vertical simulation box axis, plus three BPD. In all panels the whole system is shown.

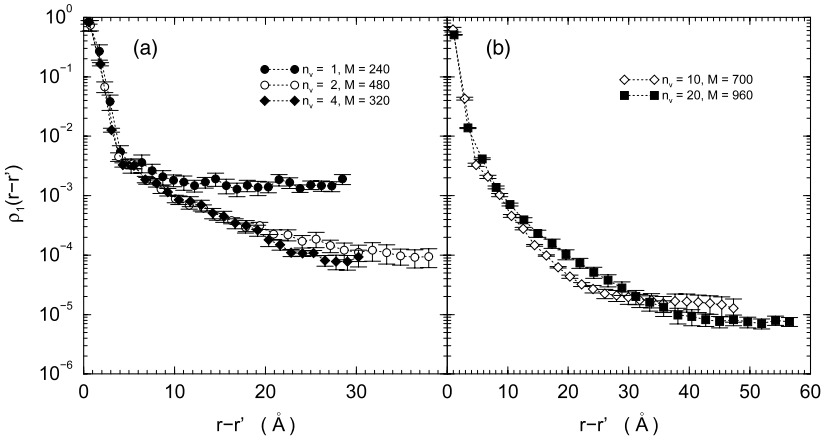

Figure 10. One-body density matrix ρ_1 computed along the first-neighbor direction in 2D ^{4}He crystals at $\rho = 0.0765$ Å^{-2} in different boxes in (a) the vacancy regime and (b) the dislocation regime.

about $(n_v \pm 2) \times a$ (a is the lattice parameter) that turns out to be comparable with $L_x/2$. This is no longer true for the box with $M = 960$, in which case ρ_1 has no ridge in the tail (see figure 12(c)).

In order to determine how the plateau of ρ_1 is affected by finite size effects one should perform computations for an even larger number of particles, but $N \simeq 10^3$ is the maximum number that we can handle currently. Another reason for studying larger systems is to establish how the number of dislocations scales with the size of the system and with the number of vacancies. Presumably supersolidity and BEC are present in a macroscopic system only if the concentration of dislocations is finite. In addition there is the question of whether the projection time τ is large enough to

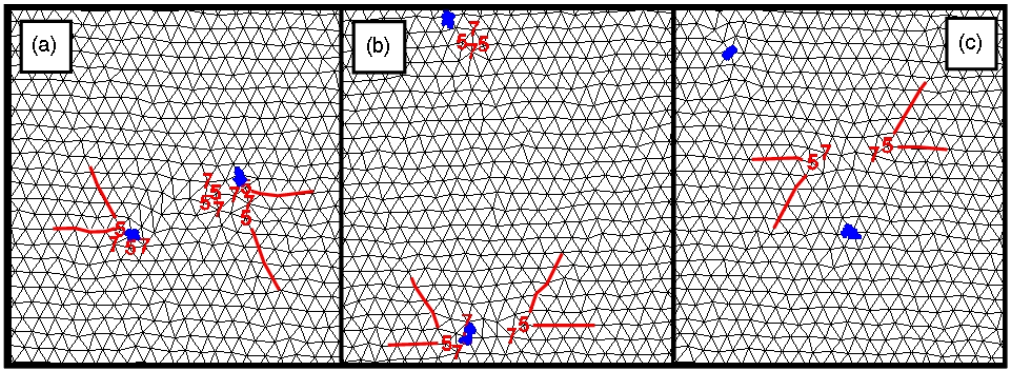

Figure 11. Delaunay triangulation of typical equilibrium configurations of a 2D ^{4}He crystal at $\rho = 0.0765$ Å^{-2} in an off-diagonal SPIGS simulation with $n_v = 20$ and $M = 960$. The bold (red) lines indicate the interrupted lines of atoms. We report the coordination number for atoms only when different from 6. The couple 5–7 indicates a dislocation core in 2D. The clump of two 5s and two 7s indicates a bound pair of dislocations [38]. The blue dots are snapshots of the half-polymers [15]. The two half-polymers are mainly found to occupy the dislocation cores like in (a), but they have also been found outside the core (both half-polymers in (c) or only one in (b)). Notice that in all panels only a small part of the full system is shown.

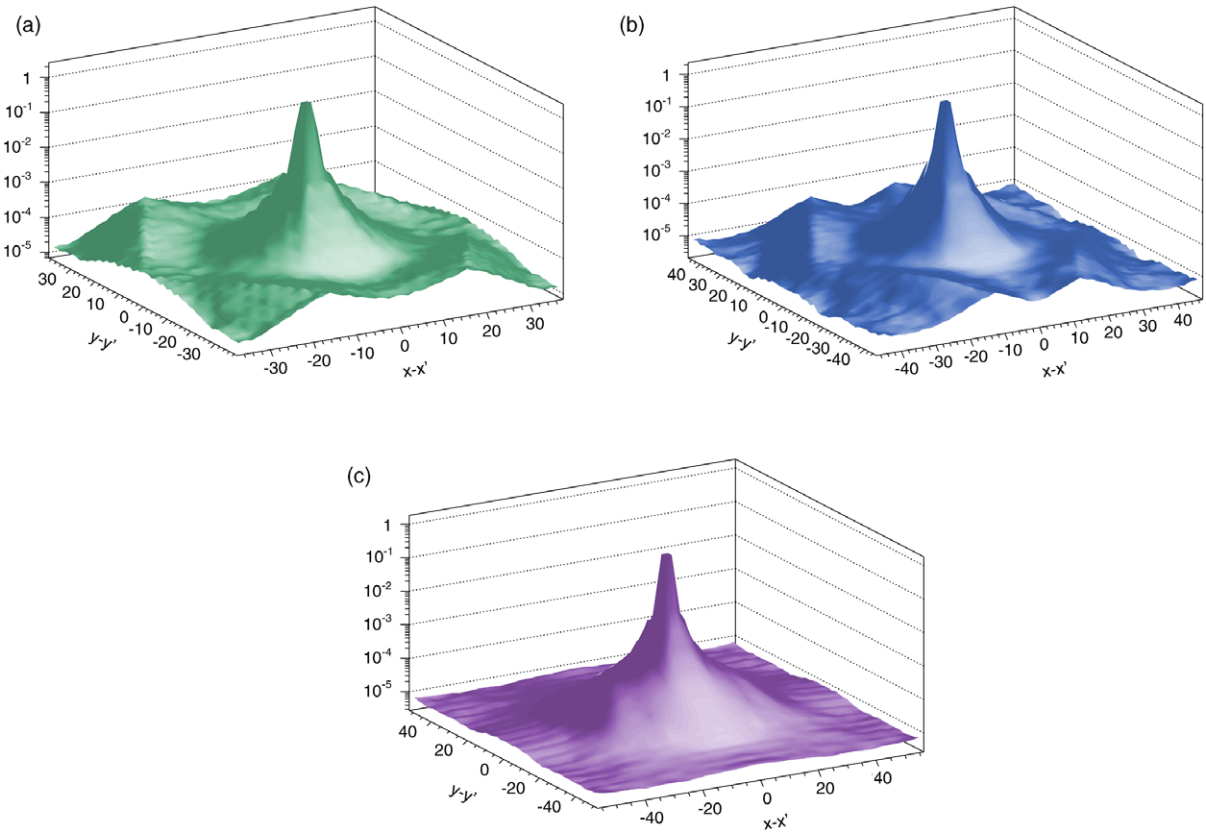

Figure 12. One-body density matrix $\rho_1(\vec{r}, \vec{r}\,')$ in the x–x', y–y' plane computed for a defected ^{4}He 2D crystal at $\rho = 0.0765$ Å^{-2}. (a) $n_v = 10$, $M = 480$; (b) $n_v = 10$, $M = 700$; (c) $n_v = 20$, $M = 960$.

have convergence to the exact result. On the basis of indirect tests performed on diagonal observables which depend on long range correlations (see figure 1) we are fairly confident that the value of τ used is large enough for getting convergence, but we are not able to provide a direct test by using a larger value of τ again because of computational limitations (a computation with $\tau = 0.775$ K^{-1} with $\delta\tau = 1/40$ K^{-1} and 10^3 atoms has to handle about 2×10^5 degrees of freedom). Our results for the dislocation regime hint that ODLRO is present, but further tests are needed in order to firmly establish this. In any case our results on off-diagonal properties of 2D systems enlighten us regarding a novel ability of dislocations in inducing exchanges even in their surroundings.

5. Conclusions

In summary, we find that crystalline order in 2D ^{4}He is stable also in the presence of a large number of vacancies and there

is no tendency to phase separation. This is true also in 3D; we have studied up to 2548 particles and 98 vacancies and in all cases we find that crystalline order is present, as shown by the presence of Bragg peaks in the static structure factor. When, in the 2D system, the number of vacancies is of order of ten and above, vacancies inserted in the initial configuration lose their identity and most of them become quantum dislocations. Such dislocations turn out to be very mobile and are able to induce exchange of particles across the system, which is necessary for supersolidity. The ability of dislocations to induce vacancies in the surrounding crystal could be relevant also for the 3D case. If this feature is confirmed for 3D, the superfluidity will be not restricted to the dislocation cores [21], and exchange processes necessary for supersolidity would be promoted by vacancies even in the bulk crystal far from dislocation cores. Simulations with numbers of particles orders of magnitude larger are needed to answer the question of whether the number of dislocation cores will increase with the system size and with the number of vacancies to give a finite concentration of dislocations able to induce ODLRO even in a macroscopic 2D ^{4}He crystal, but this is actually beyond our computational possibilities and we have to leave it for future investigations. Moreover, how much the phase correlation triggered by dislocations depends on the concentration of dislocations and its relevance for the 3D solid ^{4}He are still open questions. Our results mainly indicate that the usual concepts of commensurate or incommensurate solid, borrowed from lattice models, are not appropriate for solid helium, a system where the crystal lattice is not externally imposed, but is self-induced by the correlation among particles. In fact, the number of lattice sites M is found to be an ill defined quantity when the crystal houses many vacancies/dislocations.

We do not address the origin (intrinsic or extrinsic) of the vacancies/dislocations studied in the present paper. The issue of whether the ground state could contain zero-point defects is still debated [16, 3, 42, 43]. Our findings suggest that if the ground state of solid ^{4}He contains defects, then the Andreev–Lifshitz–Chester scenario [6, 7] would in a certain sense revive, but in terms of *ground state dislocations* rather than vacancies. On the other hand, even if the ground state has no zero-point defects, our findings suggest that in the presence of extrinsic disorder this will manifest more through fluctuating dislocations than through vacancies, at least at low T and in 2D.

Acknowledgments

This work was supported by the INFM Parallel Computing Initiative and by the Supercomputing facilities of CILEA. M Rossi would thank W Lechner for useful discussions.

References

[1] Prokof'ev N V 2007 *Adv. Phys.* **56** 381
[2] Balibar S and Caupin F 2008 *J. Phys.: Condens. Matter* **20** 173201
[3] Galli D E and Reatto L 2008 *J. Phys. Soc. Japan* **77** 111010
[4] Kim E and Chan M H W 2004 *Nature* **427** 225
Kim E and Chan M H W 2004 *Science* **305** 1941
Kim E and Chan M H W 2006 *Phys. Rev. Lett.* **97** 115302
[5] Leggett A J 1970 *Phys. Rev. Lett.* **25** 1543
[6] Andreev A F and Lifshitz I M 1969 *Sov. Phys.—JETP* **29** 1107
[7] Chester G V 1970 *Phys. Rev.* A **2** 256
[8] Scarola V W, Demler E and Das Sarma S 2006 *Phys. Rev.* A **73** 051601(R)
[9] Day J and Beamish J 2007 *Nature* **450** 853
[10] Mulders N, West J T, Chan M H W, Kodituwakku C N, Burns C A and Lurio L B 2008 *Phys. Rev. Lett.* **101** 165303
[11] Clark A C, West J T and Chan M H W 2007 *Phys. Rev. Lett.* **99** 135302
[12] Pederiva F, Chester G V, Fantoni S and Reatto L 1997 *Phys. Rev.* B **56** 5909
[13] Galli D E and Reatto L 2001 *J. Low Temp. Phys.* **124** 197
[14] Galli D E and Reatto L 2003 *Phys. Rev. Lett.* **90** 175301
[15] Galli D E and Reatto L 2003 *Mol. Phys.* **101** 1697
Galli D E and Reatto L 2004 *J. Low Temp. Phys.* **134** 121
[16] Galli D E and Reatto L 2006 *Phys. Rev. Lett.* **96** 165301
[17] Boninsegni M, Kuklov A B, Pollet L, Prokof'ev N V, Svistunov B V and Troyer M 2006 *Phys. Rev. Lett.* **97** 080401
[18] Clark B K and Ceperley D M 2008 *Comput. Phys. Commun.* **179** 82
[19] Pollet L, Boninsegni M, Kuklov A B, Prokof'ev N V, Svistunov B V and Troyer M 2008 *Phys. Rev. Lett.* **101** 097202
[20] Pollet L, Boninsegni M, Kuklov A B, Prokof'ev N V, Svistunov B V and Troyer M 2007 *Phys. Rev. Lett.* **98** 135301
[21] Boninsegni M, Kuklov A B, Pollet L, Prokof'ev N V, Svistunov B V and Troyer M 2007 *Phys. Rev. Lett.* **99** 035301
[22] Corboz P, Pollet L, Prokof'ev N V and Troyer M 2008 *Phys. Rev. Lett.* **101** 155302
[23] Soyler S G, Kuklov A B, Pollet L, Prokof'ev N V and Svistunov B V 2009 *Phys. Rev. Lett.* **103** 175301
[24] Rossi M, Vitali E, Galli D E and Reatto L 2009 *J. Phys.: Conf. Ser.* **150** 032090
[25] Liu K S and Fisher M E 1973 *J. Low Temp. Phys.* **10** 655
[26] Shibayama Y, Fukuyama H and Shirahama K 2009 *J. Phys.: Conf. Ser.* **150** 032096 and preliminary results presented by J Saunders during the Supersolid 2009 workshop in Banff
[27] Anderson P W 2008 *Phys. Rev. Lett.* **100** 215301
[28] Vitali E, Rossi M, Tramonto F, Galli D E and Reatto L 2008 *Phys. Rev.* B **77** 180505(R)
[29] Rossi M, Nava M, Reatto L and Galli D E 2009 *J. Chem. Phys.* **131** 154108
[30] Sarsa A, Schmidt K E and Magro W R 2000 *J. Chem. Phys.* **113** 1366
[31] Ceperley D M 1995 *Rev. Mod. Phys.* **67** 279
[32] Suzuki M 1995 *Phys. Lett.* A **201** 425
[33] Vitiello S A, Runge K and Kalos M H 1988 *Phys. Rev. Lett.* **60** 1970
[34] Moroni S, Galli D E, Fantoni S and Reatto L 1998 *Phys. Rev.* B **58** 909
[35] Aziz R A, Nain V P S, Carley J S, Taylor W L and McConville G T 1979 *J. Chem. Phys.* **70** 4330
[36] Vitali E, Rossi M, Reatto L and Galli D E 2009 arXiv:0905.4406
[37] Reatto L and Chester G V 1967 *Phys. Rev.* **155** 88
[38] Krishnamachari B and Chester G V 2000 *Phys. Rev.* B **61** 9677
[39] Draeger E W and Ceperley D M 2000 *Phys. Rev.* B **61** 12094
[40] Pertsinidis A and Ling X S 2001 *Nature* **413** 147
Pertsinidis A and Ling X S 2001 *Phys. Rev. Lett.* **87** 098303
[41] Lechner W and Dellago C 2009 *Soft Matter* **5** 2752
[42] Anderson P W 2009 *Science* **324** 631
[43] Rossi M, Vitali E, Galli D E and Reatto L 2008 *J. Low Temp. Phys.* **153** 250